JACS
JOURNAL OF THE AMERICAN CHEMICAL SOCIETY
Article
pubs.acs.org/JACS

Radical versus Nucleophilic Mechanism of Formaldehyde Polymerization Catalyzed by $(WO_3)_3$ Clusters on Reduced or Stoichiometric TiO_2(110)

Cristiana Di Valentin,* Massimo Rosa, and Gianfranco Pacchioni

Dipartimento di Scienza dei Materiali, Università di Milano-Bicocca, Via Cozzi 53, 20125 Milano, Italy

Supporting Information

ABSTRACT: $(WO_3)_3$ clusters deposited on the (110) rutile TiO_2 surface are excellent catalysts for the formaldehyde (CH_2O) polymerization reaction (*J. Phys. Chem. C* **2010**, *114*, 17017). The present B3LYP study unravels the possible paths of this catalyzed reaction. According to the stoichiometry of the r-TiO_2 surface, the $(WO_3)_3$ clusters can be neutral, singly charged, or doubly charged. We find that only neutral $(WO_3)_3$ and anionic $(WO_3)_3^-$ clusters are reactive toward CH_2O molecules. In both cases it is possible to determine more than one mechanism on the basis of a nucleophilic attack of the formaldehyde O atom to the W ions of the cluster. The reaction proceeds through successive attacks of other CH_2O molecules and the formation of acetal and polyacetal intermediates, which inhibits the chain propagation. Only in the case of the anionic $(WO_3)_3^-$ catalyst is a totally different reaction path possible at low temperatures. This path involves the formation of radical species where the unpaired electron is localized on the organic moiety bound to the cluster. The polymer chain propagation follows a radical mechanism with low activation barriers. Thus, a cluster's electron charging speeds up the formaldehyde polymerization at low temperatures. On the basis of these unexpected results, we conclude that electron-rich supports and low working temperatures are the keys to kinetic control of the reaction favoring a fast radical chain propagation mechanism.

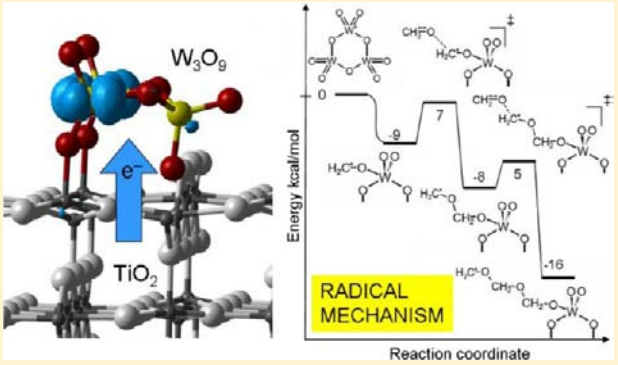

1. INTRODUCTION

Transition metal oxides are used in catalysis both as supports and as active materials directly involved in the reaction processes. Among them, tungsten trioxide (WO_3) has been widely applied and is, for example, an excellent industrial heterogeneous acidic catalyst for ethylene hydration to ethanol.[1] It was found also to accelerate other types of reactions, such as alkanes isomerization,[2] alcohols oxidation,[3] selective NO reduction,[4] and alkenes metathesis.[5] WO_3's strong Lewis acidity, which is a consequence of the nominal 6+ oxidation state of the W ions leading to a large charge/radius ratio, is highly exploited in most of the WO_3-based catalysts.

Bulk WO_3 has been observed in a large number of crystalline phases where W atoms are coordinated to six O atoms in an octahedral or slightly distorted octahedral coordination.[6] However, nanostructured WO_3 presents interesting modifications with respect to the bulk form as regards the number of defective and under-coordinated sites, the surface/volume ratio, and the electronic properties, which have strong consequences when applied in catalysis. Commonly, nanostructured metal oxides are prepared through metal evaporation in oxidizing atmosphere or through oxidation of deposited metal nanoparticles. The resulting metal oxide clusters, however, do not always present the desired dimensions and dispersions on the support. Recently, a procedure has been reported in the literature which leads to formation of regular cyclic tungsten oxide clusters $(WO_3)_3$ with well-defined structure on the (110) rutile TiO_2 surface.[7,8] Such systems are catalytically active when deposited but also in the gas phase.[9] Therefore, they are extremely appealing model systems for both experimental and computational studies.

The gaseous $(WO_3)_3$ cyclic cluster can be easily produced through direct sublimation or through laser ablation of the bulk oxide.[10,11] It presents an almost perfectly planar cyclic structure. The photoelectron spectrum[12,13] of the cluster anion provides a HOMO−LUMO gap of 3.4 eV which is very close to the amorphous tungsten oxide band gap. The adiabatic electron affinity of the $(WO_3)_3$ cluster is estimated to be between 3.45 and 3.55 eV.[12,13] Computational data reported in the literature[12−16] and based on the density functional theory (DFT) approximately reproduce these values when considering one-particle Kohn−Sham eigenvalues. Lewis acidity of $(WO_3)_3$ cluster has also been theoretically computed in terms of the reaction energy associated with addition of a fluorine anion. This is extremely high and comparable to that of a strong Lewis acid such as SbF_5.[17] From these experimental and computational studies[10−17] on the cyclic $(WO_3)_3$ cluster we learn that it

Received: May 14, 2012
Published: July 30, 2012

   dx.doi.org/10.1021/ja304661g | *J. Am. Chem. Soc.* 2012, 134, 14086−14098

is a stable species with W−O bond lengths close to those in bulk WO_3, high electron affinity, and high Lewis acidity of the W^{6+} sites. The gas-phase clusters are found to efficiently catalyze dehydration reactions of alcohols, dehydrogenation reaction of aldehydes, and ether condensation.[9,18] Activation barriers of the order of 30 kcal/mol were computed for these processes, in rather good agreement with values estimated from temperature desorption spectra.

A more efficient way to fully exploit the activity of $(WO_3)_3$ clusters, however, is heterogeneous catalysis. Heterogeneous catalysts are obtained by deposition of monodispersed or isolated $(WO_3)_3$ clusters, fully analogous to the gas-phase ones, on the (110) rutile TiO_2 surface, as proved by scanning tunneling microscopy.[7,8] DFT calculations indicate that the cluster can bind to the surface in various ways.[19] In the most stable conformations, three O atoms of the W═O type are bound to five-fold-coordinated surface Ti ions, while two W atoms form bonds with the bridging surface O atoms. The catalytic activity of these heterogeneous systems for 2-propanol dehydration and formaldehyde (CH_2O) dehydrogenation has been experimentally (in ultra-high-vacuum (UHV) conditions) and computationally investigated.[9,18,20] Reaction mechanisms are found to be analogous to the gas-phase ones, suggesting that these latter represent reasonable models of the heterogeneous catalyst.

Regarding the object of the present study, formaldehyde polymerization has been observed in UHV conditions at very low temperatures (<100 K)[20] and found to extend into the multilayers of H_2CO (up to 13 layers). The highest yield of about 50% was registered for a concentration of 1.2 $(WO_3)_3$ clusters per nm^2. This result is extremely interesting since formaldehyde, which is a fundamental building block for the synthesis of more complex organic compounds, can also be exploited for a number of copolymerization reactions with other molecules such as urea, phenol, or melamine. Its homopolymer, polyoxymetilene, has a peculiar thermal stability, is highly crystalline due to its polar nature, is stable in organic solvents, and presents good mechanical properties; thus, it is used in many applications.

The experimental data obtained so far on the formaldehyde polymerization reaction on $(WO_3)_3/TiO_2(110)$[20] do not allow for an unambiguous determination of the reaction mechanism. Also the role of the electronic and structural interplay between the $(WO_3)_3$ clusters and the TiO_2 support is not entirely clarified. The main objective of the present DFT study using the B3LYP functional[21,22] is to provide atomistic descriptions of the overall catalyst, of the polymerization reaction path, and of the role of the titania support. The work consists of three parts. First, we study the gas-phase $(WO_3)_3$ cyclic cluster in its neutral and charged states (GAUSSIAN09 suite of programs) in section 3.1.[23] Second, we investigate the overall catalyst by depositing a fixed concentration of $(WO_3)_3$ clusters on both stoichiometric and reduced (110) rutile TiO_2 surfaces, by means of periodic calculations (CRYSTAL09 code),[24] as described in section 3.2. The details of the electronic structure of the oxide/oxide interface and eventual charge transfers between the two oxides are addressed. Since the gas-phase and supported cluster properties are found to be analogous, we proceed with some important simplification of the model in the third part of the work, devoted to the catalytic reactivity (section 3.3). The polymerization reaction is modeled only on the neutral or charged gas-phase clusters, resembling neutral or charged supported clusters, except for the first step of the reaction paths which proved to be analogous for both unsupported and supported catalysts. Moreover, we restrict the study to a few propagation steps of the polymerization reaction, although this is ideally infinite. For these steps, intermediates, transition states, and products are characterized as minima or saddle points on the potential energy surface. The kinetics and thermodynamics of the multistep processes are determined in terms of enthalpies and Gibbs free energies of activation and reaction, by correcting electronic energies differences with zero-point energy, thermal, and entropic contributions.

The results of this study are rather unexpected and will pave the way to novel approaches to the catalyst preparation and experimental conditions. In fact, we have found that a reduced TiO_2 surface can easily transfer electrons to the $(WO_3)_3$ clusters. Singly charged clusters can then activate linear radical chain polymerization of formaldehyde with very low activation barriers. This reaction path competes with other paths based on the nucleophilic attack by CH_2O molecules of the W ions in the cluster, analogous to those computed for neutral $(WO_3)_3$ clusters. These paths involve the largely exothermic formation of cyclic acetals and polyacetals, which most likely inhibits chain elongation and favors small products. Low working temperature is thus the key parameter to go from thermodynamic to kinetic control favoring a radical chain propagation mechanism.

2. COMPUTATIONAL DETAILS

2.1. GAUSSIAN09 for Molecular Calculations. We carried out spin-polarized density functional calculations employing the hybrid B3LYP[21,22] scheme to describe the exchange-correlation contribution to the electron−electron interaction. All calculations have been performed employing the following basis sets (a): 6-31+G*[25] for H, C, and O; Hay−Wadt/ECP+Lanl2DZ[26] for W. Convergence tests, which will be presented in the next section, were done by comparison with calculations employing larger basis sets (b): aug-cc-pVDZ[27] for H, C, and O; the relativistic pseudopotential 60MDF+aug-cc-pVDZ-PP[28] basis set for W. The two groups of basis sets will be indicated in the rest of this article as (a) pDZ and (b) ccDZ. All geometry optimizations of intermediates and transition structures were performed without any symmetry constraint, except for the bare $(WO_3)_3$ cluster or unless specified in the text. The transition-state structures were searched by numerically estimating the matrix of the second-order energy derivatives at every optimization step and by requiring only one eigenvalue of this matrix to be negative. Critical points on the potential energy surface have been characterized by diagonalizing the Hessian matrices. Vibrational frequencies in the harmonic approximation were calculated for all optimized structures and used, unscaled, to compute zero-point energies, enthalpies, and Gibbs free energies.

2.2. CRYSTAL09 for Periodic Calculations. The periodic calculations have also been performed within spin-polarized DFT, using the hybrid B3LYP[21,22] functional, as implemented in the CRYSTAL09 code.[24] The Kohn−Sham orbitals were expanded in Gaussian-type orbitals; the all-electron or the ECP+valence-electron basis sets are, for Ti, 86411(d41); for O, 8411(d1); and for W, Hay−Wadt/ECP+311(d2).[29] The reduced TiO_2 (110) surface has been modeled by removing one oxygen atom from a stoichiometric periodic slab of five Ti layers (i.e., 15 atomic layers). This width guarantees the convergence of electronic properties.[30] A c(4×2) surface cell was used, where the minimum distance between periodically repeated images of the defect, ∼9 Å, is larger than with a p(2×2) cell of equal area. This corresponds to one vacancy every four bridging oxygens. The 2D Brillouin zone was sampled using 4 k-points. One $(WO_3)_3$ cluster was deposited per c(4×2) surface cell. Geometry optimizations were performed using the Berny algorithm, until the largest component of the ionic forces was less than 1×10^{-3} au, except for the atoms in the bottom layer which were fixed in their bulk positions.

dx.doi.org/10.1021/ja304661g | J. Am. Chem. Soc. 2012, 134, 14086−14098

Throughout this article, two energy units will be used: eV for electron affinities, band gap values, total energy differences of different conformers, and surface binding energies; and kcal/mol for reaction energies.

3. RESULTS AND DISCUSSION

3.1. Gas-Phase Neutral $(WO_3)_3$ and Anionic $(WO_3)_3^-$ and $(WO_3)_3^{2-}$ Clusters. *$(WO_3)_3$ Cluster.* The $(WO_3)_3$ cluster geometry has been optimized with both pDZ and ccDZ basis sets (see section 2.1) in order to test the convergence. The structure which presents the minimum energy has a D_{3h} symmetry. The computed structural parameters (Figure 1)

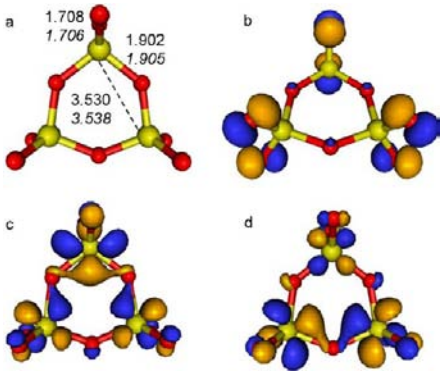

Figure 1. (a) Ball-and-stick representation of $(WO_3)_3$ neutral cluster with distances at the B3LYP/pDZ and B3LYP/ccDZ levels (bond lengths in Å). (b) HOMO and (c,d) LUMOs.

compare well with previous theoretical data in the literature.[12−16] The distance between W and bridging oxygen (O_{br}) atoms is larger than that between W and terminal oxygens (O_t), in line with the single W−O and double W═O nature of the two bonds, respectively.

The highest occupied molecular orbital (HOMO) essentially involves the O_t 2p orbitals (Figure 1). Two degenerate lowest unoccupied molecular orbitals (LUMOs) found for this cluster involve the W 5d states. The HOMO−LUMO gap from one-particle Kohn−Sham eigenvalues is the property which is the most affected by the basis set extension going from 5.43 eV for the pDZ case to 5.67 eV for the ccDZ one.

$(WO_3)_3^-$ Cluster. The vertical electron affinity of the neutral $(WO_3)_3$ cluster is 2.7 (pDZ) and 2.4 eV (ccDZ). A larger affinity is computed with the pDZ basis set because, although it contains fewer basis functions than the ccDZ one, the most external d function on W has a more diffused coefficient than in the ccDZ basis set, which allows the additional electron to be farther away, decreasing the electron−electron repulsion.

As a further step, the anion geometry is fully relaxed, removing all symmetry constraints. With the pDZ basis set, we find two stable conformers with C_1 and C_s symmetries (Figure 2a,b) which differ by 0.16 eV in energy (3.69 kcal/mol) in favor of C_s, corresponding to adiabatic electron affinities for $(WO_3)_3$ of 3.4 and 3.3 eV. This compares rather well with experimental estimates.[13] In the C_s conformer the excess electron is localized on a single W atom, while in the C_1 conformer the singly occupied molecular orbital (SOMO) involves two W atoms. With the ccDZ basis set, a third conformer was also localized which maintains the D_{3h} symmetry of the neutral cluster (Figure 2c). In this case the W−W distance is shorter than in the previous structures. The main feature of this last conformer is that the SOMO (Figure 2f) is fully delocalized on all the

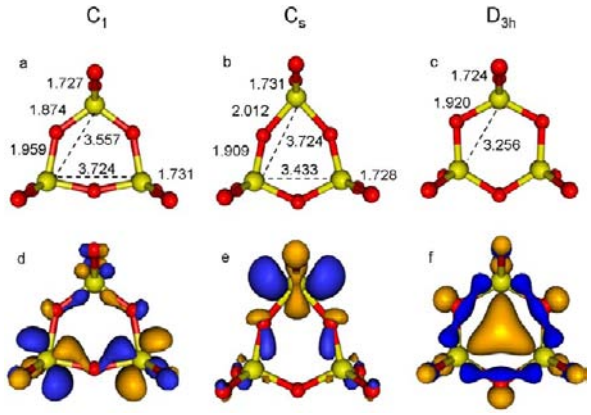

Figure 2. (a−c) Ball-and-stick representations of $(WO_3)_3^-$ anionic cluster in C_1, C_s, and D_{3h} symmetries (bond lengths in Å). (d−f) Corresponding SOMOs.

atoms of the ring, with large contributions from the W atoms. This conformer is however 0.09 eV (2.08 kcal/mol) less stable than the C_s conformer. The electron affinities computed with the ccDZ basis set are all systematically smaller by 0.3 eV than those obtained with the pDZ, for the reason discussed above.

$(WO_3)_3^{2-}$ Cluster. The addition of a second electron has also been investigated. Geometry optimization of the dianionic cluster leads to two different minima with D_{3h} and C_{2v} symmetries (see Figure 3). For the lower symmetry case, the

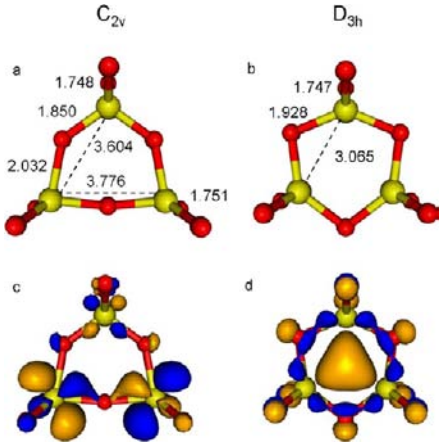

Figure 3. (a,b) Ball-and-stick representations of $(WO_3)_3^{2-}$ dianionic cluster in C_{2v} and D_{3h} symmetries (bond lengths in Å). (c,d) Corresponding HOMOs.

second adiabatic electron affinity is negative by −1.3 (ccDZ) or −1.1 eV (pDZ), indicating that the cluster cannot host a second electron. The HOMO state of the C_{2v} dianion involves only two W atoms with a node on the O_{br} in between. However, the D_{3h} conformer (ccDZ basis set) is definitely more stable (by 1.4 eV), resulting in a slightly positive second adiabatic electron affinity of 0.1 eV, in satisfactory agreement with previous CCSD(T) calculations (0.2 eV).[31] Here the HOMO hosting the two excess electrons is fully delocalized on all the atoms of the ring. This strong stabilization is described in the literature as d-type aromaticity,[12] even though this is not totally rigorous since the molecular plane should be a nodal plane of the molecular orbital. In this sense it is a σ aromaticity and not a π one.

dx.doi.org/10.1021/ja304661g | J. Am. Chem. Soc. 2012, 134, 14086−14098

For the dianionic cluster we have computed also the triplet spin configuration, since the neutral cluster has degenerate LUMOs. The two extra electrons lie on two different W atoms of the cluster. The total energy is very close to that of the C_{2v} conformer in the singlet state, differing by only 0.05 (ccDZ) or 0.07 eV (pDZ).

To summarize, similar results have been obtained for the neutral $(WO_3)_3$ cluster with the two basis sets used. For the anionic $(WO_3)_3^-$ and dianionic $(WO_3)_3^{2-}$ species, we have found that only with a larger basis set can a fully delocalized SOMO be observed maintaining the D_{3h} symmetry of the neutral cluster. Conformers with a lower symmetry have similar structural parameters with both basis sets. The first adiabatic electron affinity is better reproduced by the pDZ basis set (3.45 eV vs the experimentally determined 3.45−3.55 eV)[12,13] because, although it contains fewer basis functions, the most external one is more diffused. Moreover, it is evident that once the clusters are deposited on the TiO_2 surface, the symmetry plane is lost and therefore the D_{3h} symmetry is not compatible. These conclusions and the lower computational cost make the pDZ basis set a reasonable choice to study the cluster catalytic reactivity toward aldehyde polymerization (section 3.3.2). However, to reinforce our choice, we have also performed a preliminary study on ethanol dehydrogenation and compared the results obtained with the present setup (B3LYP/pDZ) with previously published computational and experimental data.[9] This will be discussed in further detail in section 3.3.1.

3.2. Supported $(WO_3)_3$ Clusters on the (110) Rutile TiO_2 Surface. *Stoichiometric Surface.* As a next step, we have deposited a neutral $(WO_3)_3$ cluster on the stoichiometric (110) rutile TiO_2 surface. This surface is characterized by the well-known alternating rows of under-coordinated Ti_{5c} ions and bridging O ions (O_{br}). The c(4×2) supercell slab model limits the cluster interactions with its repeated images and leads to a cluster concentration of 1.31 nm^{-2}, which is very close to that of the real experimental catalyst (1.2 nm^{-2}) producing the maximum reaction yield. Since the cluster presents both acidic and basic sites, it can interact with both surface Ti and O ions. We searched the configuration maximizing the number of interactions, which resulted in the one in Figure 4, which is consistent with previous reports.[19] Five bonds are formed: three oxygen atoms of the cluster bind to three five-fold-coordinated surface Ti ions, resulting in elongated W═O bonds (1.80−1.85 Å) with respect to those which do not interact with the surface. This is an indication that the bond order of these W═O bonds is reduced upon formation of the Ti−O covalent bonds. These can be seen as a dative bond between the basic terminal O_t ions of the cluster and the acidic Ti^{4+} sites of the surface. The other two interface bonds involve two W atoms and two surface bridging oxygens, O_{br}. Here the bonds involve the donor O_{br} sites and the acceptor W^{6+} sites. The whole interaction can thus be classified as a case of Lewis acid−base pair interactions. The cluster binding energy to the surface, with reference to an isolated cluster in the gas phase, is 3.2 eV, about 0.64 eV/bond.

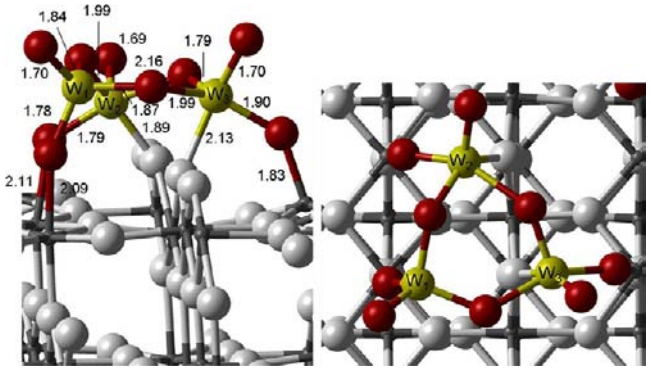

Figure 4. Side (left) and top (right) views of a $(WO_3)_3$ cluster deposited on the (110) rutile TiO_2 surface (bond lengths in Å).

The electronic structure of the catalyst was investigated in terms of the density of states (DOS, Figure S2 in Supporting Information) and their projections on the W and O atoms of the cluster, with respect to the DOS of the pristine surface. The presence of the cluster does not modify the main features of the electronic structure of TiO_2. No new states are introduced in the band gap which is unmodified (3.2 eV with the present model and setup). There is clear evidence of the covalent character of the W−O_{br} and Ti−O_t bonds from the projected DOS.

Oxygen-Deficient Surface. When the cluster is deposited on an oxygen-deficient surface the situation changes. The reduced surface is modeled by removing one O_{br} atom per supercell (0.76 vacancy per nm^2). This causes the presence of two extra electrons (triplet ground state) in the model which are localized on two specific Ti ions of the slab, a surface Ti_{5c} and a subsurface Ti_{6c} of the second triatomic layer (see spin density in Figure S1). The localization is accompanied by some structural deformation; in particular, the Ti−O bond lengths at the Ti^{3+} centers are longer (2.02−2.08 Å). This result is qualitatively similar to what we found some years ago[32] for a four-triatomic-layers model, although in that case both Ti^{3+} species were in the first layer of the slab. The energy difference to trap the electron on different Ti ions is very small. The electronic structure is also very similar to that reported before, with two new peaks below the bottom of the conduction band (1.1 and 1.5 eV). The lowest energy corresponds to the Ti^{3+}_{6c} site which has a stronger trapping character than ions on the top layer.

After deposition of the $(WO_3)_3$ cluster, the surface oxygen vacancy is filled by one O from the cluster. In this configuration only three bonds are formed between the cluster and the surface, involving three O_t atoms of the cluster, two surface Ti_{5c} ions, and the two under-coordinated Ti ions of the O vacancy (Figure 5). Singlet and triplet spin configurations in their optimized (almost identical) structures are very close in energy (0.05 eV in favor of the singlet). The binding energy of the cluster in the ground-state spin configuration is 2.2 eV, which is by far smaller than that for the pristine surface, as a consequence of the reduced number of bonds.

Two practically degenerate solutions are found for the triplet spin configuration: One case (Figure 5, right bottom panel) corresponds to the transfer of two electrons from the Ti^{3+} ions of the surface to the W^{6+} ions of the cluster; this is very similar to what was found in the singlet closed-shell calculation where the same charge transfer is found and the two electrons are coupled in a molecular orbital involving mainly 5d states of two W atoms. In the second triplet solution (Figure 5, left bottom panel), only one electron is transferred to a W ion in the cluster, the second one remaining on one Ti^{3+} ion of the surface. This result indicates that the second electron affinity of $(WO_3)_3$ remains negligible also on the TiO_2 support and that there is no additional electrostatic stabilization of the dianion due to the interaction with the cationic sites of the surface. The

dx.doi.org/10.1021/ja304661g | J. Am. Chem. Soc. 2012, 134, 14086−14098

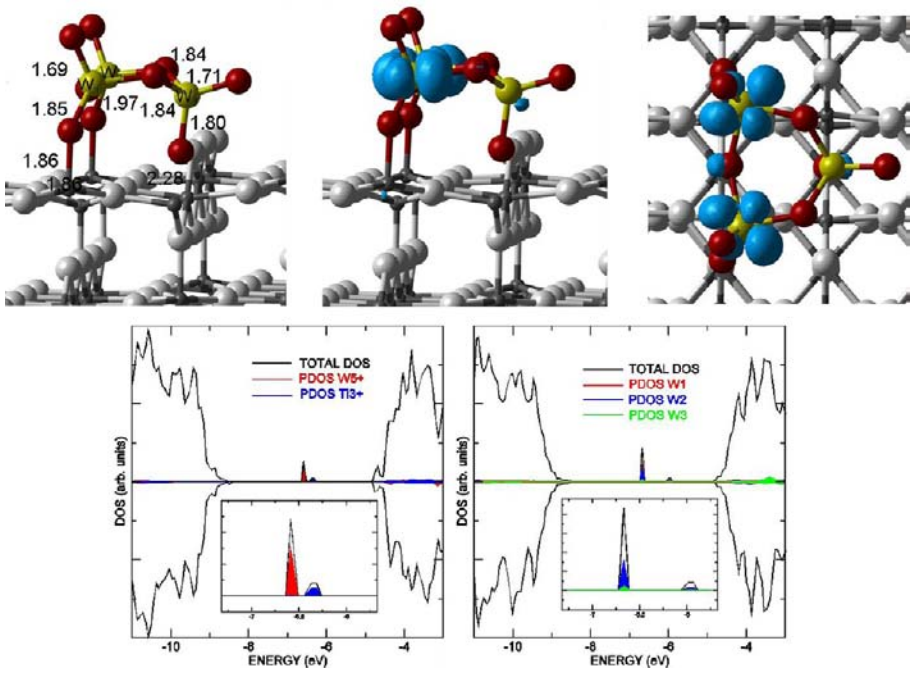

Figure 5. Top: side (left and center) and top (right) views of the $(WO_3)_3$ cluster deposited on the oxygen-deficient (110) rutile TiO_2 surface (bond lengths in Å). Spin density plots of the triplet solution with two electrons transferred to $(WO_3)_3$. Bottom: DOS with the projections on W or Ti^{3+} centers for the two triplet solutions: one electron (left) and two electrons (right) transferred to the $(WO_3)_3$ cluster.

peaks associated with the W^{5+} and Ti^{3+} states are highly localized at 1−1.5 eV below the bottom of the conduction band in the DOS of the overall $(WO_3)_3/TiO_2$ catalyst (Figure 5, left bottom panel).

From these results the role of defects such as oxygen vacancies in the TiO_2 support is clear, as these defects can substantially modify the donor or acceptor properties of the supported $(WO_3)_3$ cluster. A negatively charged cluster will be a favorable substrate for electrophilic reactions. In the model used in this study, we have a 1:1 cluster-to-vacancy ratio. For a real catalyst it is reasonable to suppose a lower concentration of defects and therefore a single electron transfer to the supported cluster $(WO_3)_3^-$.

3.3. Catalytic Reactivity. Computational modeling of the catalyst reactivity involves optimization of a considerable number of intermediates and transition-state structures. Therefore, since the computational cost to treat the surface +cluster system is very high, we need to rely on some assumptions and to introduce some simplifications. On the basis of the above discussion (section 3.2) one can safely conclude that the deposition of the cluster on a stoichiometric TiO_2 surface does not alter in a major way its electronic properties. In particular, due to the absence of net charge transfer from or to the surface, we expect the acidic properties of the W atoms to remain largely unaltered. Structural deformations upon cluster deposition are not so large as to preclude molecular adsorption. Indeed, we have checked that the binding of an aldehyde molecule to gas-phase and supported $(WO_3)_3$ clusters is similar, as discussed in detail in the last paragraph of section 3.3.2 (see below). Thus, in the following, we assume that the reactivity of $(WO_3)_3/TiO_2$ can be reasonably studied even in the absence of the support. Of course, this neglects the possible involvement of sites at the cluster/surface boundary in the reaction and other constraints due to the presence of the solid surface.

In the case of a defective surface, we observe the transfer of one or two excess electrons from the Ti^{3+} species of the support to the $(WO_3)_3$-adsorbed cluster, resulting in the formation of one or two W^{5+} centers. For the singly charged supported species, the electron localization is the same as observed in the gas-phase anionic $(WO_3)_3^-$ cluster (see pDZ results in section 3.1). Also geometrical parameters of the supported and unsupported anionic clusters are very similar. On this basis we make the assumption that the catalyst reactivity can be reasonably investigated by studying the unsupported $(WO_3)_3^-$ cluster.

The dianionic $(WO_3)_3^{2-}$ cluster has not been further considered in relation to the formaldehyde reactivity because the excessive negative charge totally inhibits formaldehyde nucleophilic attack to the W ions of the cluster.

3.3.1. Ethanol Dehydrogenation Reaction. In order to verify the reliability of the chosen computational setup (pDZ basis set), we have performed a preliminary study of the ethanol dehydrogenation reaction in the gas phase. This has been experimentally and computationally investigated before,[9] thus providing a benchmark for our approach. The very good agreement with previous results and the reasonably good agreement with the experimental data confirm the validity of the adopted computational setup (see the Supporting Information, section S.3).

3.3.2. Formaldehyde Polymerization Reaction. Catalysis by $(WO_3)_3$ Cluster. The reactivity of formaldehyde is essentially directed by the electrophilic character of the C atom or the nucleophilic character of the O atom. Formaldehyde polymerization can be initiated by opening the double bond with a cationic or an anionic mechanism. In general, formaldehyde polymerization takes place through an anionic mechanism; therefore, we have first considered the possibility of a nucleophilic attack of the C atom, as sketched in the top part of Scheme 1.

dx.doi.org/10.1021/ja304661g | J. Am. Chem. Soc. 2012, 134, 14086−14098

Scheme 1

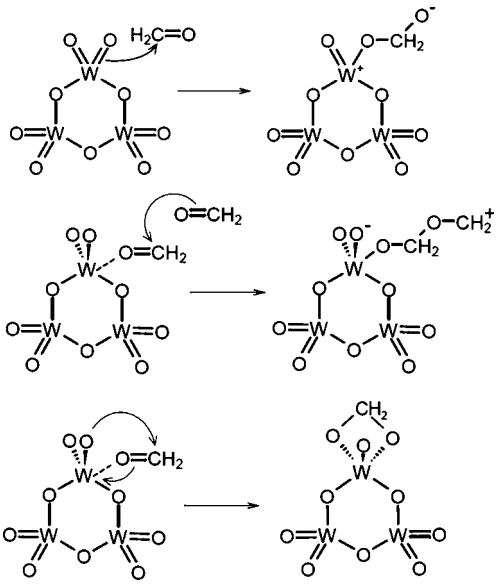

However, this attempt was totally unsuccessful, which suggested that the mechanism is most likely a cationic one. In fact, as already mentioned, the W atoms in the cluster are characterized by a strong Lewis acidity. The formaldehyde molecule can bind to the W atoms through a coordinative bond with the carbonyl O atom. Since when supported on the (110) rutile surface the cluster plane (passing through the three W atoms) is parallel to the surface, we have initially directed the approach of the formaldehyde molecule to the cluster from one side of this plane. This leads to the coordination of the carbonyl O atom to all three W atoms of the cluster (see Figure 6, **1b**).

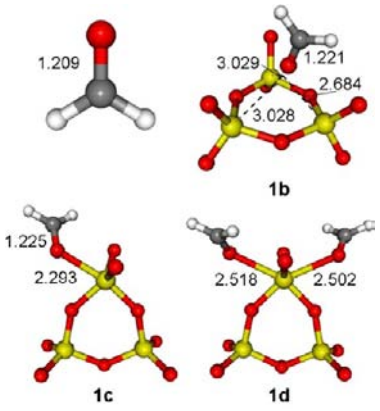

Figure 6. Ball-and-stick representation of the isolated and interacting formaldehyde molecule CH_2O with a neutral $(WO_3)_3$ cluster (bond lengths in Å).

The interaction is rather weak, as proven by the long distances (more than 3 Å), with a binding energy of 11.9 kcal/mol. However, if we allow the molecule to coordinate to only one W atom (see Figure 6, **1c**), the coordinative bond becomes much shorter (2.29 Å), with a binding energy of 15.7 kcal/mol. The C═O bond is slightly elongated in both configurations. It is possible to coordinate a second H_2CO molecule to the same W atom (Figure 6, **1d**). The average binding energy per molecule becomes only 8.8 kcal/mol.

The reaction mechanism was studied starting from both intermediates **1b** and **1c**. We first investigated a nucleophilic attack of a second formaldehyde molecule to the C atom of the first adsorbed one for the intermediate **1b** (central part of Scheme 1). However, during the optimization the newly formed C−O bond breaks. In a second attempt, we considered that the nucleophilic attack to the same C atom is done by the O of the nearby W═O group in **1b**, forming a cyclic acetal (**3b**, Figure 7 or bottom part of Scheme 1) through the transition

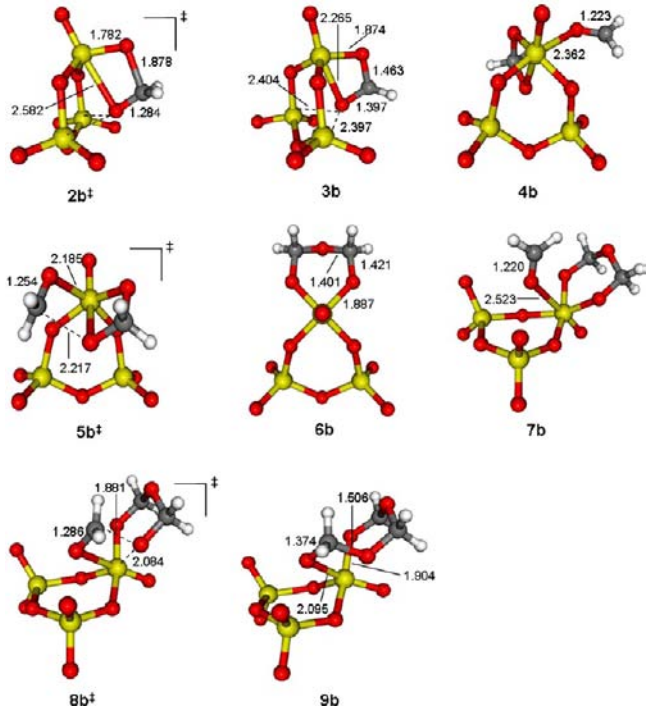

Figure 7. Ball-and-stick representation of intermediates and transition structures of the reaction path catalyzed by the neutral $(WO_3)_3$ cluster, starting from species **1b**, reported in Figure 8 (bond lengths in Å).

state **2b**‡, with an activation barrier of 8.9 kcal/mol. The reaction coordinate is characterized by the new O−C bond formation, together with pyramidalization at the carbon center. The acetal is not a stable species; in fact, the process is endothermic and costs 2.0 kcal/mol. The acetal presents two different W−O bond distances because one of the O atoms also interacts with the other two W ions in the cluster. As a next step, we tried the nucleophilic attack of the C in the acetal by the O of a second CH_2O molecule. This prefers to bind to the W atom, instead, forming the intermediate **4b** (Figure 7) with an energy gain of 12.1 kcal/mol. It then reacts with one O of the acetal group through an electrophilic attack of the carbonyl C atom. The activation barrier for this concerted step (**5b**‡) is 11.2 kcal/mol. The acetal O involved in the reaction is the one with a longer distance to the W ion. In the resulting intermediate **6b**, the formaldehyde dimer is bound to the cluster as a cyclic 6-term polyacetal (Figure 7). The process is exothermic by 17.0 kcal/mol, and the two W−O bond distances are equivalent. In order to obtain the trimer, a similar mechanism takes place. A third formaldehyde molecules binds to the same W ion of the cluster, intermediate **7b** in Figure 7. The process is thermodynamically favored by 15.0 kcal/mol. Direct formation of the trioxane from **7b** would require breaking of the C═O bond and concomitant formation of two

dx.doi.org/10.1021/ja304661g | J. Am. Chem. Soc. 2012, 134, 14086−14098

C−O bonds with the O atoms of the polyacetal. We could not localize any structure like that. On the contrary, it was possible to localize a transition structure for the nucleophilic attack of one acetal O to the carbonyl C atom (**8b**‡), with an activation barrier of 13.8 kcal/mol. This is the highest barrier computed so far for this reaction path and would therefore be the rate-determining step. The intermediate formed (**9b**) is again a cyclic polyacetal where one of the two terminal oxygens of the chain binds to all three cluster W ions. The process from **7b** to **9b** is endothermic by 9.6 kcal/mol. The intermediate **7b** is more stable, probably because the 6-member ring in a chair conformation is less sterically hindered than the 8-member ring in **9b**.

On the basis of these results, it is plausible that formaldehyde polymerization proceeds through the following steps: each formaldehyde molecule initially coordinates to the W metal center and then undergoes a nucleophilic attack to its C atom, leading to the addition of a new unit to the polymer. For the reaction path starting from intermediate **1b** we have limited the search to the initialization step and the first two propagation steps, as described above. The overall reaction path is described in Figure 8. From **1b** to **9b** the process is exothermic by 44.4

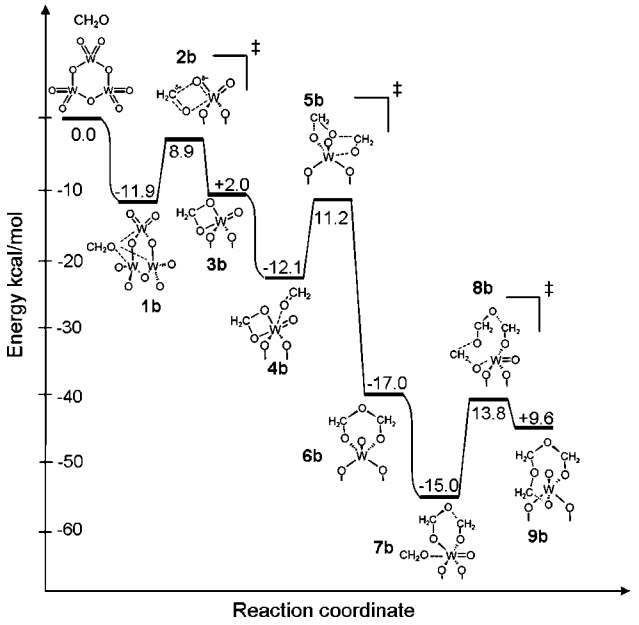

Figure 8. Scheme of the reaction path of formaldehyde polymerization catalyzed by the neutral $(WO_3)_3$ cluster starting from intermediate **1b**. Reaction energies and activation barriers from total electronic energy differences are reported (electronic energies in Table 1).

kcal/mol. The activation barrier of the rate-determining step is 13.8 kcal/mol. **7b** is the most stable intermediate along the reaction path. We cannot exclude that the system may further evolve toward oligomers of larger molecular size. We also note that, in all the intermediates and transition structures, only one W═O group is involved in the coordination of acetals. Thus, these species can analogously form when the cluster is supported on the TiO_2 surface, where only three W═O bonds are used to bond to the surface while the remaining ones are free.

Gibbs free energy differences have been obtained from the vibrational analysis (Table 1). Large variations can be observed with respect to electronic energy differences related to the entropic term in the cases of **1b** and **7b** intermediates formation. In these two processes the number of gas-phase units is reduced from two to one with a high entropic cost due to the reduction in the degree of freedom.

The reaction path starting from intermediate **1c**, where the first CH_2O is coordinated only to one W atom of the cluster, has also been investigated (Figures 9 and 10). Analogously to the reaction path from **1b**, activation of the formaldehyde molecule is achieved through coordination with one W atom followed by formation of an acetal. However, it is possible to observe some differences in the conformations of the intermediates and transition structures which affect the relative stability. While the energy cost to form the acetal is only slightly larger than before (3.7 vs 2.0 kcal/mol), the activation barrier to obtain this intermediate is about 10 kcal/mol higher. This is a strong indication that the preliminary coordination of the molecule to only one W atom is less efficient than the coordination to three W atoms as in **1b**. The second coordination involves three W atoms and results in a larger stabilization energy (13.7 kcal/mol) and a smaller activation barrier (9.1 kcal/mol) for the nucleophilic attack by one acetal O. The resulting intermediate **6c**, with a 6-member-ring polyacetal, is characterized by two different W−O bonds, due to double coordination of one acetal O atom to two W atoms. The trimer species is formed after coordination of a third molecule (**7c**). Then one acetal oxygen attacks the electrophilic carbon of the third molecule through **8c**‡, leading to the intermediate with an 8-member-ring polyacetal, **9c**. Here there is an important difference with respect to the previous reaction path because the process is now exothermic by 9.7 kcal/mol. However, the activation barrier is slightly higher: 14.4 kcal/mol.

Another difference is that for this reaction path we have been able to advance a few steps more and see the formation of a 1,3,5-trioxane, first coordinated to the cluster (**11c**) and then desorbed. The activation barrier from **9c** to **11c** is very high: 33 kcal/mol. Probably there is some intermediate step that we could not identify, which is also supported by the very different structures of **9c** and **10c**‡. The last steps of the reaction path are endothermic. The overall reaction, from gas-phase cluster and three CH_2O molecules to production of trioxane, is an exothermic process by 30.7 kcal/mol (electronic energy difference). After correction to the enthalpy difference at 298 K, we obtain −22.26 kcal/mol, which underestimates the experimental value of −33.27 kcal/mol. The Gibbs free energy difference (Table 2), after correction for the entropic term, is positive by 3.06 kcal/mol. The Gibbs free energy differences to form intermediates **1c**, **4c**, and **7c** are tiny because of the entropic reduction associated with the transition from a gas-phase to an adsorbed molecule.

We can now summarize the results on the polymerization reaction involving neutral $(WO_3)_3$ clusters. We have computed two reaction mechanisms which are representative of possible reaction paths. Other paths can be conceived where the formaldehyde molecules may coordinate to different W atoms at the various propagation steps, or where the polyacetal binds to the cluster with different conformations than those considered here. However, we do not expect large differences in the energy profiles. In the mechanisms considered here, the polymerization starts with the formation of a relatively unstable 4-member cyclic acetal and proceeds with the activation of additional molecules through coordination to the same W atom. The activation of the formaldehyde can be described as a cationic mechanism; however, looking at the mechanism in

dx.doi.org/10.1021/ja304661g | J. Am. Chem. Soc. 2012, 134, 14086−14098

Table 1. Reaction Energies and Activation Barriers in Terms of Energies, Enthalpies, and Gibbs Free Energies for the Reaction Path Reported in Figure 8

species	electronic energy (Ha)	ZPE (Ha)	thermal corrections, 298 K (kcal/mol)	S, 298 K (cal/mol)	ΔE with ZPE (kcal/mol)	ΔH, 298 K (kcal/mol)	ΔG, 298 K (kcal/mol)
$(WO_3)_3$	−880.97906	0.031107	28.64	128.2	0	0	0
CH_2O	−114.50709	0.026770	18.60	52.2	0	0	0
1b	−995.50897	0.060654	49.45	145.0	−12.57	−12.70	−2.12
2b‡	−995.49478	0.062672	49.28	131.0	10.17	8.73	12.92
3b	−995.50585	0.064772	50.55	130.4	4.54	3.06	7.43
4b	−1110.03217	0.094542	71.52	149.5	−12.57	−10.29	−15.99
5b‡	−1110.01420	0.094390	70.87	146.0	11.06	10.51	11.56
6b	−1110.06131	0.097916	73.21	153.5	−16.17	−16.59	−17.79
7b	−1224.59225	0.127997	94.10	162.3	−12.89	−13.27	−0.31
8b‡	−1224.57020	0.130225	94.11	149.0	15.23	13.85	17.80
9b	−1224.57703	0.132521	95.61	151.0	12.39	11.06	14.42

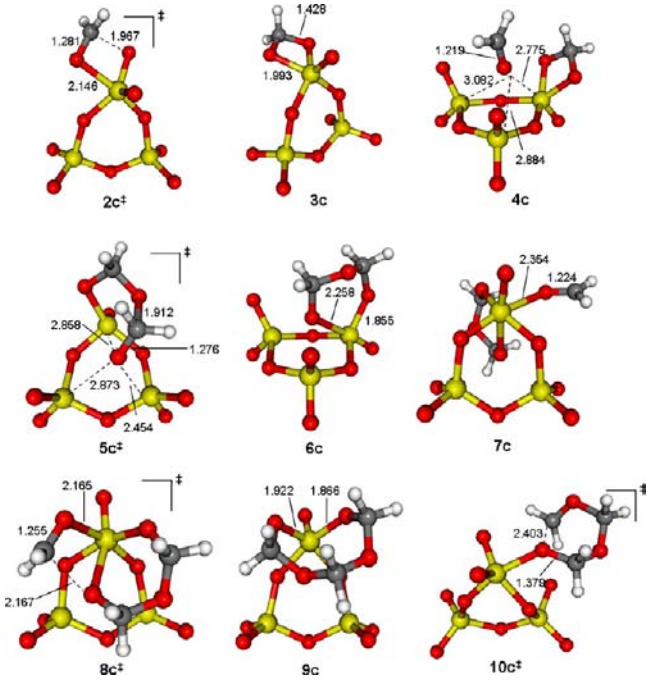

Figure 9. Ball-and-stick representation of intermediates and transition structures of the reaction path catalyzed by the neutral $(WO_3)_3$ cluster, starting from species **1c**, reported in Figure 10 (bond lengths in Å).

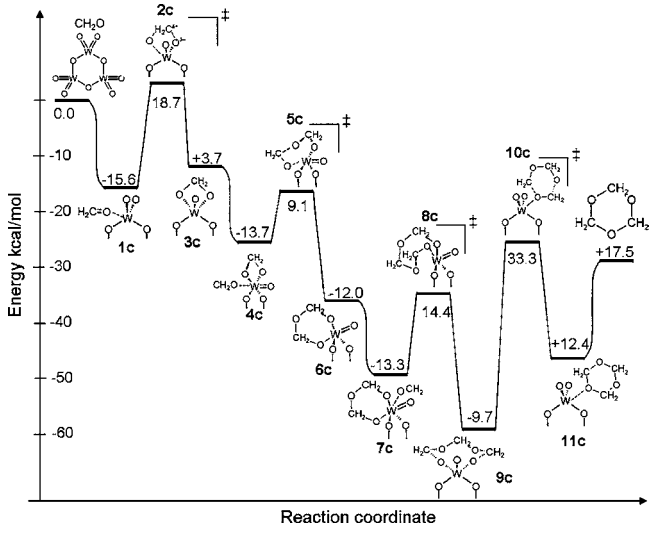

Figure 10. Scheme of the reaction path of formaldehyde polymerization catalyzed by the neutral $(WO_3)_3$ cluster starting from intermediate **1c**. Reaction energies and activation barriers from total electronic energy differences are reported (electronic energies in Table 2).

detail, one realizes that the W atoms enhance the electrophilic character of the C atom of each additional formaldehyde molecule, as a consequence of the fact that at each propagation step a site for adsorption is made free. From a thermodynamic point of view, the two mechanisms differ in the energetics of the addition of the third molecule, which costs 9.6 kcal/mol in the first mechanism and is exothermic in the second one. From the kinetic point of view, the two mechanisms have different rate-determining steps with a slightly lower value of activation Gibbs free energy for the first mechanism (17.80 vs 19.40 kcal/mol), if we exclude the last step of chain termination, which we computed only for the second mechanism. The experimental temperature at which the chain propagation has been observed is lower than 100 K, corresponding to a very low activation barrier for the rate-determining step, which is not compatible with the values computed so far.

Catalysis by $(WO_3)_3^-$ Cluster. We have seen that the presence of electron-rich defects on the TiO_2 surface can lead to the formation of negatively charged supported clusters. Thus, it is intriguing to see whether an excess electron can modify the reactivity in formaldehyde polymerization. When deposited on the TiO_2 surface, the $(WO_3)_3^-$ negative cluster presents the electron fully localized on a single W ion, as a consequence of the symmetry breaking upon adsorption. Therefore, we have considered a gas-phase model where the extra charge is also localized on one W ion in a 5+ formal oxidation state. The first formaldehyde molecule has the possibility to bind to either a W^{6+} or a W^{5+} (see **1e** and **1f**, respectively, in Figure 11).

The adduct **1e** is very similar to those calculated for the neutral cluster, even though the negative charge weakens the bond between the O from C═O and the W atom. The binding energy is only 4.5 kcal/mol, vs 11.9 and 15.7 kcal/mol reported for intermediates **1b** and **1c** in the previous section (Figure 6). In contrast, in the intermediate **1f** the W^{5+}−OCH_2 bond is the shortest and the C═O is the longest computed so far, indicating a stronger interaction, with a binding energy of 8.6 kcal/mol. This result is rather unexpected since reduction to W^{5+} should reduce the Lewis acidity of the W center. A closer look at the molecular orbitals and, in particular, the SOMO of the adduct can help in rationalizing the result. In intermediate

dx.doi.org/10.1021/ja304661g | J. Am. Chem. Soc. 2012, 134, 14086−14098

Table 2. Reaction Energies and Activation Barriers in Terms of Energies, Enthalpies, and Gibbs Free Energies for the Reaction Path Reported in Figure 10

species	electronic energy (Ha)	ZPE (Ha)	thermal corrections, 298 K (kcal/mol)	S, 298 K (cal/mol)	ΔE with ZPE (kcal/mol)	ΔH, 298 K (kcal/mol)	ΔG, 298 K (kcal/mol)
$(WO_3)_3$	−880.97907	0.03111	128.25	28.6			
CH_2O	−114.50709	0.02677	52.25	18.6			
1c	−995.51115	0.06132	146.07	49.6	−13.52	−13.87	−3.61
2c‡	−995.48132	0.06094	140.95	48.8	18.48	17.87	19.40
3c	−995.50518	0.06392	140.80	50.5	5.37	4.61	6.19
4c	−1110.03419	0.09310	158.13	71.2	−12.24	−12.21	−1.80
5c‡	−1110.01964	0.09618	140.87	71.6	11.06	9.45	14.59
6c	−1110.05333	0.09904	139.50	73.3	−8.28	−9.93	−4.37
7c	−1224.58164	0.12915	155.00	94.3	−11.22	−11.51	−0.55
8c‡	−1224.55875	0.12915	150.38	93.6	14.36	13.69	15.06
9c	−1224.59703	0.13215	154.52	95.7	−7.77	−8.33	−8.18
10c‡	−1224.54389	0.12869	159.11	93.9	31.17	31.56	30.19
11c	−1224.57768	0.13197	167.91	96.1	12.02	12.59	8.60
$(CH_2O)_3$	−343.570237	0.09912	71.83	65.4	−18.92	−22.26	3.06

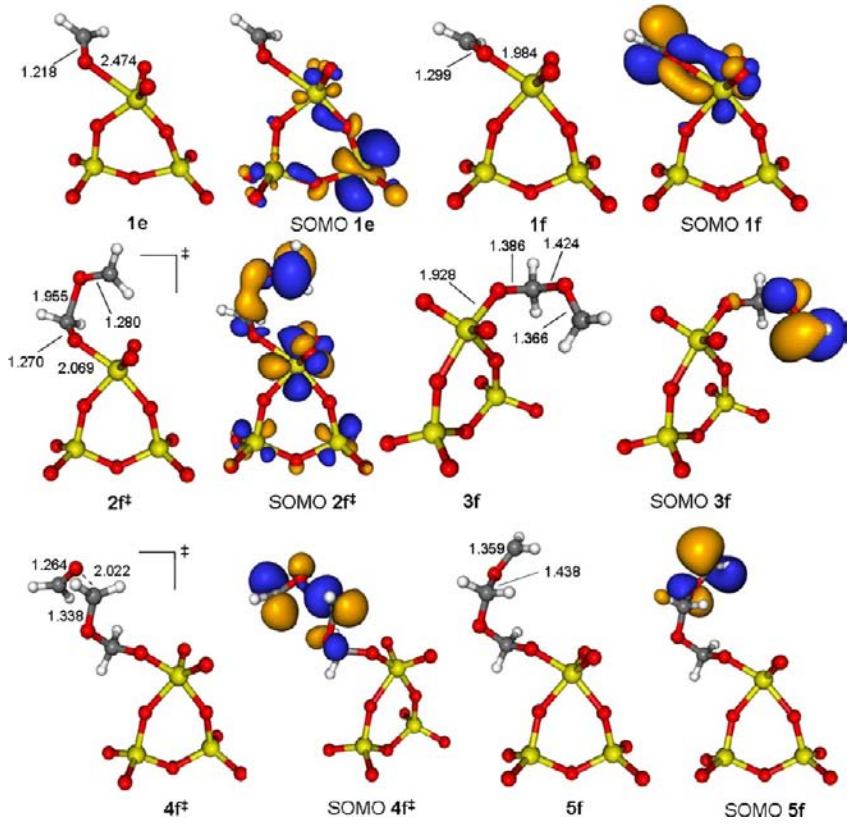

Figure 11. Ball-and-stick representation of intermediates and transition structures of the reaction path catalyzed by the anionic $(WO_3)_3^-$ cluster, starting from species **1f**, reported in Figure 12 (bond lengths in Å).

1f the SOMO is the result of the overlap between the originally unoccupied π^* orbital of the CH_2O molecule and the singly occupied $5d_{xz}$ state of the W^{5+} ion. The SOMO has a π-type binding character, which justifies the spin delocalization from the W ion to the C atom of the molecule (0.2 electron on W and 0.8 electron on C). This result is extremely important: coordination of a formaldehyde molecule to a $(WO_3)_3^-$ radical anion produces a partial radical on the C atom of the molecule, having of course crucial consequences on the reactivity and on the reaction path of the polymerization. We expect that intermediate **1e** will give a reactivity very similar to that described in the previous section; therefore, we concentrate on the reaction path starting from intermediate **1f** (radical mechanism).

The presence of an unpaired electron on the C atom suggests that the process can proceed through a radical chain mechanism. This type of polymerization is typical for double-bond compounds such as olefins, but not for carbonyl species such as aldehydes. However, in the present context it is the electron-rich cluster $(WO_3)_3^-$ which initializes the radical process by an electron transfer to the C atom in the formaldehyde molecule. The reaction path in this case does not involve cyclic intermediates, as observed in the previous section. The radical species formed are relatively stable, and the

dx.doi.org/10.1021/ja304661g | J. Am. Chem. Soc. 2012, 134, 14086−14098

reaction proceeds with the addition of a further formaldehyde molecule and radical propagation along the chain. A second CH_2O molecule interacts with the intermediate **1f**, forming a new C−O bond where the C atom is that of the first molecule in **1f** and the O atom is that of the second attacking molecule (Figure 12). The activation barrier of this step is 7.2 kcal/mol,

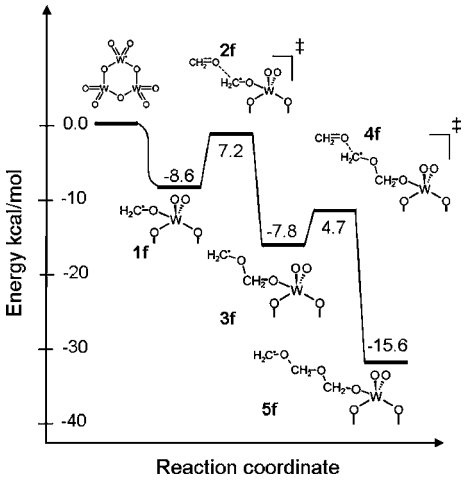

Figure 12. Scheme of the reaction path of formaldehyde polymerization catalyzed by the anionic $(WO_3)_3^-$ cluster starting from intermediate **1f**. Reaction energies and activation barriers from total electronic energy differences are reported (electronic energies in Table 3).

and in the resulting product, **3f**, a new C−O bond is formed and the extra electron is in a π^* orbital of the added CH_2O, mostly on the terminal C atom (see Figure 11). This first step involves the breaking of a π bond with formation of a σ bond and an overall energy release of 7.8 kcal/mol. Starting from intermediate **3f** and going through the transition state **4f**‡, a third formaldehyde molecule is then attached to the chain (**5f**). The barrier is smaller than for the first step (4.7 kcal/mol) because the unpaired electron in intermediate **3f** is in a π^* and not a π orbital as in intermediate **1f**. The reaction is accompanied by an energy release of 15.6 kcal/mol. In intermediate **5f**, analogously to intermediate **3f**, the unpaired electron is essentially on the terminal C atom of the chain; thus, the propagation can proceed with the repetition of steps similar to the ones just described. The overall formation of a 3-member chain is an exothermic process by 32.0 kcal/mol.

From a thermodynamic point of view and considering total electronic energy differences, the radical chain propagation is less favorable than that computed in the previous section for closed-shell systems. On the contrary, activation barriers are lower, which better reconciles with the experimentally observed low reaction temperatures. For all the computed radicals, the S^2 value is close to 0.75, with no spin contamination from high multiplicity spin states.

Looking at Gibbs free energy differences at 298 K (Table 3), the overall picture changes dramatically. The reaction steps become somewhat endergonic (2.85 and 6.76 kcal/mol) or only slightly exergonic (−1.44 kcal/mol). The activation Gibbs free energies for the steps from **1f** to **3f** and from **3f** to **5f** are 20.76 and 16.32 kcal/mol, respectively. Thus, at room temperature the species produced through the radical process are very unstable and the barriers to chain propagation become high and comparable to those for the closed-shell systems discussed in the previous section.

We want now to consider the possibility that the radical at the C position in intermediate **1f** undergoes an intramolecular attack to the O of the cluster W═O group (activation barrier of 15.6 kcal/mol), forming a 4-member cyclic acetal (**2g**, Figure 13). The difference between **2g** and **2b** is the presence of an

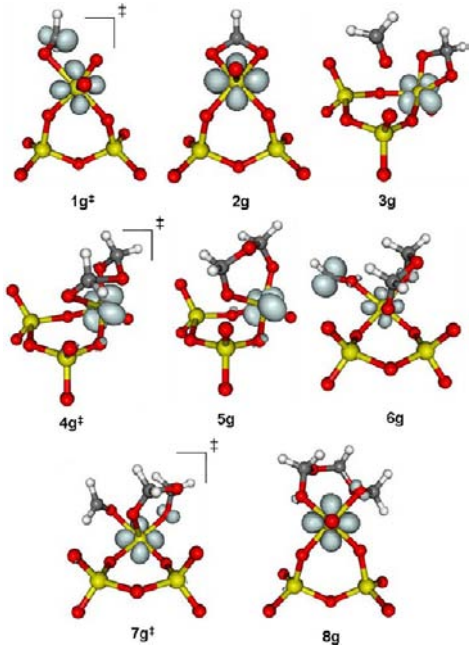

Figure 13. Ball-and-stick representation and spin density plot of intermediates and transition structures of the reaction path catalyzed by the anionic $(WO_3)_3^-$ cluster, starting from species **2g**, reported in Figure 14.

extra electron on W ion and a 3 kcal/mol energy difference in the barrier. The process to form **2g** is exothermic by 13.6 kcal/

Table 3. Reaction Energies and Activation Barriers in Terms of Energies, Enthalpies, and Gibbs Free Energies for the Reaction Path Reported in Figure 12

species	electronic energy (Ha)	ZPE (Ha)	thermal corrections, 298 K (kcal/mol)	S, 298 K (cal/mol)	ΔE with ZPE (kcal/mol)	ΔH, 298 K (kcal/mol)	ΔG, 298 K (kcal/mol)
$(WO_3)_3^-$	−881.10596	0.02936	137.53	27.9			
CH_2O	−114.50709	0.02677	52.25	18.6			
1f	−995.62917	0.05815	148.91	47.9	−8.85	−9.33	2.85
2f‡	−1110.12471	0.08895	161.45	68.7	9.77	8.92	20.76
3f	−1110.14818	0.09152	164.52	70.4	−3.33	−4.16	6.76
4f‡	−1224.64777	0.12082	180.92	90.5	6.29	5.63	16.32
5f	−1224.68015	0.12540	180.94	93.0	−11.16	−12.12	−1.44

dx.doi.org/10.1021/ja304661g | J. Am. Chem. Soc. 2012, 134, 14086−14098

mol, indicating that W^{5+} formation is more convenient than a radical on the formaldehyde C atom. However, the kinetic barrier to form **2g** is higher than that to attack a second CH_2O molecule (**2f**, 7.2 kcal/mol).

In order to establish the effect of a negative charge on the nonradical reactivity, the reaction path starting from intermediate **2g** has been investigated. The mechanism involves intermediates which are analogous to those found in the previous section. The chain propagation takes place through coordination and activation of a second formaldehyde molecule and nuclephilic attack of the O from the acetal to the electrophilic C. The spin density plots show that the extra electron is always located on the W^{5+} ion, except for intermediate **6g**. We can conclude that the reaction mechanism is not affected by the presence of the extra electron. However, differences exist in the energy profile (Figure 14).

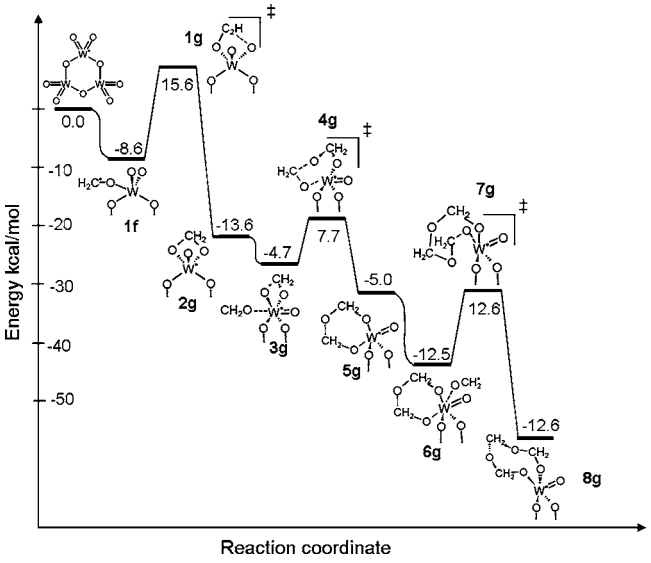

Figure 14. Scheme of the reaction path of formaldehyde polymerization catalyzed by the anionic $(WO_3)_3^-$ cluster starting from intermediate **2g**. Reaction energies and activation barriers from total electronic energy differences are reported (electronic energies in Table 4).

At odds with the closed-shell system, here the formation of the 4-member cyclic acetal (**2g**) is exothermic (Table 4). The adsorption of the second CH_2O molecule here is only 4.7 kcal/mol (instead of −12.1/−13.7 kcal/mol for **4b** and **4c**), because of the different W oxidation state. The activation barriers are slightly lower than those in the corresponding reaction profile for the neutral cluster (Figures 8 and 10). Going to Gibbs free energies at 298 K, we observe that the processes become endergonic or only slightly exergonic (**1f**, **3g**, **6g**), similarly to our observations for closed-shell systems.

It is possible to envisage other reaction paths involving formation of cyclic polyacetals, rather than the simplest acetal **2g** just discussed. In the Supporting Information we report two other examples (section S.4): (1) starting from the intermediate **3f** with two CH_2O units we considered the formation of a cyclic polyacetal bound to the cluster, as observed in case of the neutral $(WO_3)_3$ cluster, and (2) starting from the intermediate **5f** with three CH_2O units we considered the formation of a 8-member cyclic polyacetal. However, the mechanism and the energetics of these processes are analogous to those found for **2g** and for the corresponding paths with the neutral cluster. Therefore, they do not stand as a relevant alternative for a more favorable or faster polymerization reaction path.

To conclude and summarize this section, we expect that, under thermodynamic control, the reaction path will probably be analogous to that described in Figure 14 (or Figure S6), since a large energy release is associated with the cyclization steps, while under kinetic control (low temperatures) the polymerization reaction occurs through a radical chain mechanism thanks to lower activation barriers (Figure 12).

Catalysis by Gas-Phase vs Supported Clusters. It is important to link the results obtained for the gas-phase clusters to the real catalyst case where the $(WO_3)_3$ species are supported on the TiO_2 surface. With this aim and due to the high computational cost, only a few selected calculations were performed. In particular, the first step of the aldehyde polymerization reaction, i.e., the binding of the first molecule, was investigated for the supported clusters on a stoichiometric surface and on a reduced TiO_2 surface. These findings are then compared to the results for the neutral and anionic gas-phase species (**1c** and **1f**), respectively. The analogy is evident since the binding modes are the same (see models in Figure 15 and compare them with **1c** in Figure 6 and **1f** in Figure 11) with bond energies of 7.6 and 4.8 kcal/mol. Most importantly, the spin density distribution associated with the unpaired electron in the case of the radical intermediate is essentially the same in the unsupported cluster, **1f**, and in the supported cluster, Figure 15 (left side). These results prove (i) that the catalytic

Table 4. Reaction Energies and Activation Barriers in Terms of Energies, Enthalpies, and Gibbs Free Energies for the Reaction Path Reported in Figure 14

species	electronic energy (Ha)	ZPE (Ha)	thermal corrections, 298 K (kcal/mol)	*S*, 298 K (cal/mol)	Δ*E* with ZPE (kcal/mol)	Δ*H*, 298 K (kcal/mol)	Δ*G*, 298 K (kcal/mol)
(WO_3)	−881.10596	0.02936	137.53	27.9			
CH_2O	−114.50709	0.02677	52.25	18.6			
1f	−995.62917	0.05815	148.91	47.9	−8.85	−9.33	2.85
1g‡	−995.60426	0.05879	142.63	47.6	16.03	15.38	17.25
2g	−995.65078	0.06285	141.04	49.9	−10.61	−11.53	−9.19
3g	−1110.16544	0.09146	159.00	70.4	9.59	−3.43	6.80
4g‡	−1110.15320	0.09446	143.81	70.7	9.56	7.97	12.50
5g	−1110.17341	0.09780	143.00	72.7	−1.02	−2.66	2.11
6g	−1224.70041	0.12625	156.87	92.5	−11.44	−11.88	−0.44
7g‡	−1224.68035	0.12629	159.38	92.5	12.61	12.57	11.82
8g	−1224.71983	0.13041	161.86	94.9	−9.57	−9.83	−11.31

dx.doi.org/10.1021/ja304661g | J. Am. Chem. Soc. 2012, 134, 14086−14098

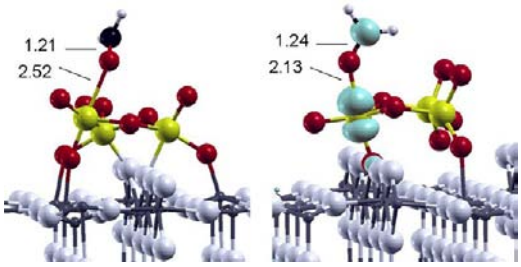

Figure 15. Left: one aldehyde molecule bound to the $(WO_3)_3$ cluster supported on the stoichiometric rutile TiO_2 surface. Right: one aldehyde molecule bound to the $(WO_3)_3$ cluster supported on the reduced rutile TiO_2 surface with spin density plot. Bond lengths in Å.

processes on supported and unsupported clusters start from similar intermediates and (ii) that the radical process is totally feasible for clusters supported on reduced TiO_2 surfaces as well as for anionic gas-phase species.

4. CONCLUSIONS

We have investigated the structural and electronic properties of $(WO_3)_3$ clusters in the gas phase or supported on stoichiometric or reduced TiO_2 (110) surfaces. While on stoichiometric TiO_2 the $(WO_3)_3$ cluster is bound via direct Ti−O or W−O covalent bonds without net electron transfer, on the reduced surface, obtained by creating O vacancies, there is a net electron transfer from the Ti^{3+} ions of TiO_2 to $(WO_3)_3$. This is related to the high electron affinity of gas-phase $(WO_3)_3$. Both $(WO_3)_3^-$ and $(WO_3)_3^{2-}$ clusters can form on r-TiO_2 by means of this mechanism, but for relatively high surface coverage the presence of the $(WO_3)_3^-$ radical anion is most likely. The properties of neutral and charged $(WO_3)_3$ gas-phase or supported clusters are similar. Based on this consideration and on the clear evidence that, for the first step of the aldehyde polymerization reaction, the intermediates with one molecule bound to a gas-phase neutral or anionic cluster (**1c** and **1f**) are similar to those for clusters supported on a stoichiometric or a reduced TiO_2 surface, respectively, we have simulated the complex reactivity of $(WO_3)_3$ using the gas-phase species only. While this is evidently a crude approximation, it allows us to clearly identify the effect on the reaction mechanism of the extra charge localized on the supported cluster, and indirectly the role played by the support. Of course, other effects, such as possible reaction mechanisms involving sites at the interface between $(WO_3)_3$ and TiO_2, are not taken into account.

We have investigated a considerable number of reaction paths, starting from either neutral or charged $(WO_3)_3$ catalysts. In both cases it is possible to determine a number of mechanisms based on a nucleophilic attack of the O atom of the formaldehyde molecule to the W ions of the cluster. The reaction proceeds though successive attacks of other molecules and through formation of acetal and polyacetal intermediates. This actually inhibits the chain propagation. However, on the $(WO_3)_3^-$ radical anion a totally different reaction path is possible with lower activation barriers at low temperatures. This path involves the formation of radical species where the unpaired electron is localized on the organic moiety. The polymer chain propagation can easily take place through a radical mechanism. We conclude that electron charging of the cluster has a beneficial effect on the kinetics of the formaldehyde polymerization reaction which speeds up the process at low temperature. Electron-rich supports and low working temperatures are the key parameters to induce the kinetic control of the reaction, thus favoring a fast radical chain propagation mechanism.

The conclusions drawn from this study are relevant for many other reactions catalyzed by $(WO_3)_3/TiO_2(110)$, besides the one here considered. More generally, this study suggests novel opportunities for the exploitation of interface charge transfers between extended supports and supported clusters in catalytic processes.

■ ASSOCIATED CONTENT

Supporting Information

Oxygen-deficient (110) rutile surface; DOS of neutral $(WO_3)_3$ deposited on stoichiometric (110) rutile surface; ethanol dehydrogenation reaction; additional reaction paths of formaldehyde polymerization reaction catalyzed by $(WO_3)_3^-$ cluster. This material is available free of charge via the Internet at http://pubs.acs.org.

■ AUTHOR INFORMATION

Corresponding Author

cristiana.divalentin@mater.unimib.it

Notes

The authors declare no competing financial interest.

■ ACKNOWLEDGMENTS

This work is supported by CARIPLO Foundation through the Advanced Materials Grant 2009 “Development of second generation photocatalysts for energy and environment”, by the Italian MIUR through the FIRB Project RBAP115AYN “Oxides at the nanoscale: multifunctionality and applications” and the PRIN Project “New generation photosensitive semiconducting oxides modified with non metals to enhance solar light harvesting. Design, synthesis, characterisation and testing”, by Regione Lombardia and CILEA Consortium, through a LISA Initiative (Laboratory for Interdisciplinary Advanced Simulation).

■ REFERENCES

(1) Chu, W.; Echizen, T.; Kamiya, Y.; Okuhara, T. *Appl. Catal. A: Gen.* **2004**, *259*, 199.
(2) Wilson, R. D.; Barton, D. G.; Baertsch, C. D.; Iglesia, E. J. *J. Catal.* **2000**, *194*, 175.
(3) Martin, C.; Solana, G.; Malet, P.; Rives, V. *Catal. Today* **2003**, *78*, 365.
(4) Lietti, L.; Alemany, J.; Forzatti, P.; Busca, G.; Ramis, G.; Giamello, E.; Bregani, F. *Catal. Today* **1995**, *29*, 143.
(5) Grunert, W.; Feldhaus, R.; Anders, K.; Sphiro, E. S.; Minachev, K. M. J. *J. Catal.* **1989**, *120*, 444.
(6) Collaboration: Authors and editors of the volumes III/17G-41D: *WO_3: crystal structure, general remarks.* Madelung, O., Rössler, U., Schulz, M. (ed.). SpringerMaterials - The Landolt-Börnstein Database (http://www.springermaterials.com). DOI: 10.1007/10681735_669.
(7) Kim, J.; Bondarchuk, O.; Kay, B. D.; White, J. M.; Dohnalek, Z. *Catal. Today* **2007**, *120*, 186.
(8) Bondarchuk, O.; Huang, X.; Kim, J.; Kay, B. D.; Wang, L. S.; White, J. M.; Dohnalek, Z. *Angew. Chem., Int. Ed.* **2006**, *45*, 4786.
(9) Kim, Y. K.; Rousseau, R.; Kay, B. D.; White, J. M.; Dohnàlek, Z. *J. Am. Chem. Soc.* **2008**, *130*, 5059.
(10) Bergowitz, J.; Chupka, W. A.; Inghram, M. G. *J. Chem. Phys.* **1957**, *27*, 85.
(11) Azens, A.; Kitembergs, M.; Kanders, U. *Vacuum* **1995**, *7*, 745.

(12) Huang, X.; Zhai, H. J.; Kiran, B.; Wang, L. S. *Angew. Chem., Int. Ed.* **2005**, *44*, 7251.
(13) Huang, X.; Zhai, H. J.; Li, J.; Wang, L. S. *J. Phys. Chem. A* **2006**, *110*, 85−92.
(14) Sun, Q.; Rao, B. K.; Jena, P.; Stoltic, D.; Kim, Y. D.; Gantefor, G.; Castelman, A. W. *J. Chem. Phys.* **2004**, *121*, 19.
(15) Li, S.; Dixon, D. A. *J. Phys. Chem. A* **2006**, *110*, 6231.
(16) Li, S.; Dixon, D. A. *J. Phys. Chem. C* **2011**, *115*, 39.
(17) Martin, J. M. L.; Sundermann, A. *J. Chem. Phys.* **2001**, *114*, 3408.
(18) Kim, Y. K.; Dohnàlek, Z.; Kay, B. D.; Rousseau, R. *J. Phys. Chem. C* **2009**, *113*, 9721.
(19) Zhu, J.; Jin, H.; Zang, L. L.; Li, Y.; Zhang, Y.; Ding, K.-N.; Huang, X.; Ning, L.; Chen, W.-K. *J. Phys. Chem. C* **2009**, *113*, 17509−17517.
(20) Kim, J.; Kay, B. D.; Dohnalek, Z. *J. Phys. Chem. C* **2010**, *114*, 17017.
(21) Becke, A. D. *J. Chem. Phys.* **1993**, *98*, 5648.
(22) Lee, C.; Yang, W.; Parr, R. G. *Phys. Rev. B* **1988**, *37*, 785−789.
(23) Frisch, M. J.; Trucks, G. W.; Schlegel, H. B.; Scuseria, G. E.; Robb, M. A.; Cheeseman, J. R.; Scalmani, G.; Barone, V.; Mennucci, B.; Petersson, G. A.; Nakatsuji, H.; Caricato, M.; Li, X.; Hratchian, H. P.; Izmaylov, A. F.; Bloino, J.; Zheng, G.; Sonnenberg, J. L.; Hada, M.; Ehara, M.; Toyota, K.; Fukuda, R.; Hasegawa, J.; Ishida, M.; Nakajima, T.; Honda, Y.; Kitao, O.; Nakai, H.; Vreven, T.; Montgomery, Jr., J. A.; Peralta, J. E.; Ogliaro, F.; Bearpark, M.; Heyd, J. J.; Brothers, E.; Kudin, K. N.; Staroverov, V. N.; Kobayashi, R.; Normand, J.; Raghavachari, K.; Rendell, A.; Burant, J. C.; Iyengar, S. S.; Tomasi, J.; Cossi, M.; Rega, N.; Millam, J. M.; Klene, M.; Knox, J. E.; Cross, J. B.; Bakken, V.; Adamo, C.; Jaramillo, J.; Gomperts, R.; Stratmann, R. E.; Yazyev, O.; Austin, A. J.; Cammi, R.; Pomelli, C.; Ochterski, J. W.; Martin, R. L.; Morokuma, K.; Zakrzewski, V. G.; Voth, G. A.; Salvador, P.; Dannenberg, J. J.; Dapprich, S.; Daniels, A. D.; Farkas, Ö.; Foresman, J. B.; Ortiz, J. V.; Cioslowski, J.; Fox, D. J. *Gaussian 09*, Revision A.1; Gaussian, Inc.: Wallingford, CT, 2009.
(24) Dovesi, R.; Saunders, V. R.; Roetti, C.; Orlando, R.; Zicovich-Wilson, C. M.; Pascale, F.; Civalleri, B.; Doll, K.; Harrison, N. M.; Bush, I. J.; D'Arco, Ph.; Llunell, M. *CRYSTAL09*; University of Torino: Torino, Italy, 2009.
(25) Ditchfield, R.; Hehre, W. J.; Pople, J. A. *J. Chem. Phys.* **1971**, *54*, 724. Clark, T.; Chandrasekhar, J.; Spitznagel, G. W.; Schleyer, P. v. R. *J. Comput. Chem.* **1983**, *4*, 294−301. Frisch, M. J.; Pople, J. A.; Binkley, J. S. *J. Chem. Phys.* **1984**, *80*, 3265−3269.
(26) Hay, P. J.; Wadt, W. R. *J. Chem. Phys.* **1985**, *82*, 270−284.
(27) Kendall, R. A.; Dunning, T. H., Jr.; Harrison, R. J. *J. Chem. Phys.* **1992**, *96*, 6796−6806.
(28) Figgen, D.; Peterson, K. A.; Dolg, M.; Stoll, H. *J. Chem. Phys.* **2009**, *130*, 164108.
(29) www.crystal.unito.it
(30) Bredow, T.; Giordano, L.; Cinquini, F.; Pacchioni, G. *Phys. Rev. B* **2004**, *70*, 035419.
(31) Li, S.; Dixon, D. A. *J. Phys. Chem. A* **2007**, *111*, 11093.
(32) Di Valentin, C.; Pacchioni, G.; Selloni, A. *Phys. Rev. Lett.* **2006**, *97*, 166803.